

This is the post-print version of the following article: *Di Silvio, D; Martínez-Moro, M; Salvador, C; de los Angeles Ramirez, M; Rocio Caceres Velez, P; Grazia Ortore, M; Dupin, D; Andreozzi, P; Moya, SE., [Self-assembly of poly\(allylamine\)/siRNA nanoparticles, their intracellular fate and siRNA delivery](#), Journal of Colloid and Interface Science, 2019, 557 (757-766)*

DOI: [10.1016/j.jcis.2019.09.082](https://doi.org/10.1016/j.jcis.2019.09.082)

This article may be used for non-commercial purposes in accordance with Elsevier Terms and Conditions for Self-Archiving.

# Self-assembly of poly(allylamine)/siRNA

## nanoparticles, their intracellular fate and siRNA delivery

*Desirè Di Silvio,<sup>a</sup> Marta Martínez-Moro,<sup>a</sup> Cristian Salvador,<sup>a,b</sup> Maria de los Angeles Ramirez,<sup>a,c</sup> Paolin Rocio Caceres Velez,<sup>a</sup> Maria Grazia Ortore,<sup>d</sup> Damien Dupin<sup>b</sup> Patrizia Andreozzi,<sup>\*a</sup> and Sergio E. Moya<sup>\*a</sup>*

<sup>a</sup> CICbiomaGUNE - Soft Matter Nanotechnology Group, Paseo Miramón nº 182, Edificio C, 20014 Donostia-San Sebastián, Spain

<sup>b</sup> CIDETEC Nanomedicine, Paseo Miramón, 196, 20014 Donostia-San Sebastián, Spain

<sup>c</sup> Instituto de Nanosistemas, Universidad Nacional de San Martín (INS-UNSAM), Av. 25 de Mayo 1021, San Martín, Buenos Aires, Argentina

<sup>d</sup> Dipartimento di Scienze della Vita e dell'Ambiente, Università Politecnica delle Marche, Ancona, Italy.

Keywords: siRNA Delivery, Polyamine Complexes, Intracellular Fate, Fluorescence Cross-Correlation Spectroscopy.

## ABSTRACT:

Silencing RNA (siRNA) technologies attract significant interest as a therapeutic tool for a large number of diseases. However, the medical translation of this technology is hampered by the lack of effective delivery vehicles for siRNAs in cytosol that prevent their degradation in the bloodstream. The use of molecular complexes based on polyamines have great potential for siRNA delivery as polyamines can protect the siRNA during circulation and at the same time favor siRNA translocation in cytosol. Here, nanoparticles are prepared by complexation of poly(allylamine hydrochloride) (PAH) and siRNA varying the ratio of nitrogen groups from PAH to phosphate groups from siRNA (N/P ratio). Nanoparticles are characterized by transmission electron microscopy and dynamic light scattering. The stability of complexes of green rhodamine labelled PAH (G-PAH) and Cy5 labelled siRNA (R-siRNA) at different pHs and in cell media is studied by fluorescence cross-correlation spectroscopy (FCCS). FCCS studies show that the nanoparticles are stable at physiological pH and in cell media but they disassemble at acidic pH. An optimal N/P ratio of 2 is identified in terms of stability in media, degradation at endosomal pH and toxicity. The intracellular fate of the complexes is studied following uptake in A549 cells. The cross-correlation between G-PAH and R-siRNA decreases substantially 24 h after uptake, while diffusion times of siRNA decrease indicating that the complexes disassemble, liberating the siRNAs. The release of siRNAs into the cytosol is confirmed with parallel confocal laser scanning microscopy. Flow cytometry studies show that PAH/siRNA nanoparticles are effective at silencing green fluorescent protein expression at low N/P ratios at which polyethylenimine/siRNA shows no significant silencing.

## 1. Introduction

Small interfering or silencing RNA (siRNA) technologies are based on the inhibition of gene expression or translation by siRNAs targeting messenger RNA.[1] siRNA technologies have great potential for the treatment of a wide variety of diseases,[2] ranging from cancer[3–6] to viral infections[7,8] and brain disorders.[9,10] Despite their medical potential, the clinical translation of siRNA technologies has up to now been limited. This limited progress is due in part to the difficulties of delivering siRNAs *in vivo*. Unprotected siRNAs are easily degraded in the bloodstream, and siRNAs alone do not translocate across cell membranes.[11] In addition, it has been reported that siRNAs can be immunogenic.[12] Therefore, siRNAs must be delivered with an appropriate vehicle that protects siRNAs from nuclease action and at the same time triggers intracellular uptake.[13,14] Until now, the best agents for siRNA delivery are cationic lipids and polycations, i.e. polyelectrolytes bearing multiple positive charges.[15,16] The negatively charged siRNAs associate with the positively charged lipids or polycations through electrostatic interactions, and in some cases, through hydrogen bonding to form molecular complexes. Positive charges in both lipids and polycations come from amines that are usually primary or quaternary.[17] Amines are also responsible for inducing the passage of the complexes to the cell interior as they easily disrupt cell membranes.[14] When siRNA complexes have translocated in the endosomes, the complexes should degrade, and the siRNAs should be released to ensure that silencing will take place. It is important to bear in mind that the efficacy of silencing will not only depend on the uptake of siRNA complexes but also on their stability as complexes must disassemble to release the siRNAs following cellular uptake.[18] The intracellular fate of the liposome/siRNA and polycation/siRNA

complexes is a largely unknown aspect of siRNA delivery, as it is not easy to trace the individual components, siRNAs and lipids or polymer, individually in cells.

Fluorescence correlation spectroscopy (FCS) and fluorescence cross-correlation spectroscopy (FCCS) techniques provide a means to trace the fate of both the complexes and their individual components. FCS is a spectroscopic technique used to study the diffusion time of fluorescent molecules and objects in different matrixes, including cells.[19] In FCS, fluctuations in the intensity of fluorescence coming from molecules or objects in nanomolar concentration are recorded inside a femtoliter confocal volume. Diffusion times are derived from the correlation analysis of the fluctuations in fluorescence intensity.[20] FCCS, a variation of FCS, studies the dynamic interactions between two molecules or objects labeled with spectroscopically different dyes.[21,22] FCCS provides the time correlation between two fluorescent objects in the confocal volume. The technique has been widely applied to study protein-protein interactions inside live cells,[23–27] and to analyze the association of oligonucleotides and polymers both in bulk solution and in cells.[28–30]

Polyethylenimine (PEI) is probably the most frequently used polycation in gene delivery; however, other polycations have shown potential for applications in therapy.[31] In a recent paper we explored the formation of phosphate-poly(allylamine hydrochloride) (PAH) nanoparticles complexing siRNAs. PAH is a polycation displaying primary amines and PAH-phosphate nanoparticles carrying siRNAs were successful in silencing green fluorescent protein (GFP) in GFP-A549 cells.[32] The phosphate ions interact with the amines of PAH and act as crosslinkers. siRNAs were entrapped in the nanoparticles following different procedures from complexes of PAH and siRNAs, by adding siRNAs

after particle formation and by mixing PAH with siRNA and phosphate in one step. However, the PAH/siRNA complexes themselves form nanoparticles without adding phosphate ions and could also be used for silencing as an alternative to PEI/siRNA nanoparticles. Since PAH displays only primary amines and these interact very strongly with the phosphate groups of siRNAs at neutral pHs we expected that the ratio of amines from PAH to phosphate of siRNA (N/P) for the formation of stable and effectively silencing PAH/siRNA complexes would be lower than for PEI/siRNA complexes. Moreover, the complexation of the primary amines with the phosphate groups should be weaker at endosomal pH, as phosphate groups lose charges, liberating the siRNA and at the same time the protonation of the amines groups of PAH at this pH should create an osmotic swelling in the endosomes, facilitating siRNA translocation and ultimately the silencing by the siRNAs. For these reason PAH/siRNA nanoparticles could be an interesting alternative to PEI/siRNA in certain applications, requiring lower N/P for an effective silencing.

In this paper we aimed to study PAH/siRNA nanoparticles focusing on their physical characterization and their biological fate *in vitro*. These aspects are fundamental for siRNA delivery and we tackle the potential use of PAH/siRNA nanoparticles in silencing strategies. We applied the gel retardation assay, transmission electron microscopy (TEM), and dynamic light scattering (DLS) to study the formation of PAH/siRNA complexes and their structural changes depending on the nitrogen/phosphate molar ratio (N/P ratio). To gain further understanding of the mechanism of siRNA delivery, we investigated the complexation and stability of PAH/siRNA nanoparticles first *in vitro* and then intracellularly by FCS and FCCS. Biological fate and intracellular translocation of the PAH/siRNA nanoparticles was also studied by FCS/FCCS and confocal laser scanning

microscopy (CLSM). Fate studies revealed that PAH/siRNA nanoparticles have a dynamic nature, which is influenced by the ratio of PAH to siRNA and the environmental conditions. Free siRNA was detected after 24 h, indicating dissociation of the nanoparticles. From our results it is possible to estimate the time scale for the disassembly of PAH/siRNA complexes inside the cell, which is a fundamental component for evaluating the efficacy of siRNA delivery and gene silencing. Finally, we show that PAH/siRNAs are effective in silencing GFP expression in A549 cells at low N/P ratios, where PEI/siRNAs do not show effective silencing.

## 2. Experimental Section

### 2.1. Materials

Poly(allylamine hydrochloride) salt (PAH) ( $15 \times 10^3$  g/mol), Cy5-siRNA, hydrochloric acid (HCl), and sodium hydroxide (NaOH) were purchased from Sigma-Aldrich, USA. PAH labeled with green rhodamine (G-PAH) was provided by Surflay AC, Germany. Human lung adenocarcinoma cell lines (A549 CCL185) were obtained from the American Type Culture Collection (ATCC), USA. UltraPure DNase/RNase-Free Distilled Water and Nunc™ Lab-Tek™ Chambered Cover glass were purchased from ThermoFisher Scientific, USA. RPMI 1640 medium was purchased from Lonza, USA. HyClone™ fetal bovine serum (FBS) was purchased from ThermoFisher Scientific, USA, and penicillin and streptomycin from Sigma Aldrich, USA. RPMI medium without phenol red and Leibovitz's L-15 medium without phenol red were purchased from ThermoFisher Scientific, USA.

### 2.2. Methods

#### 2.2.1. Formation of PAH/siRNA Nanoparticles

PAH/siRNA nanoparticles were prepared in a one-step procedure by mixing PAH (17.5 kDa) and siRNA (13 KDa) at different nitrogen/phosphate (N/P) molar ratios, from 1 to 50, in RNase-free water at room temperature, **Fig. 1A**.<sup>[33]</sup> We refer to the nanoparticles in terms of the N/P ratio, which is the ratio of protonatable polymer amine groups to nucleic acid phosphate groups.<sup>[33,34]</sup> Nanoparticles were prepared over a range of N/P ratios from 1 to 40 using concentrations of 1-10  $\mu$ M PAH and 0.1-2  $\mu$ M siRNA. Nanoparticle formation is driven by the electrostatic and hydrogen bonding interactions between the amines of PAH and the phosphate groups of siRNA.<sup>[32]</sup>

#### 2.2.2. Fluorescence Cross-Correlation Spectroscopy (FCCS)



FCCS was performed with a Zeiss LSM 880 confocal microscope. Image acquisition and analysis were controlled by Zen black software. GaASP and PMTr detectors for single fluorescence molecule detection and dynamic characterization were used. Measurements were performed with a Zeiss C-Apochromat 40x, numerical aperture 1.2 water immersion objective. For FCCS in live cells, two simultaneous fluorescence channel detection coupled with transmission T-PMT was used. Fluorescence emission was detected in the range of 500-560 nm and 650-710 nm. Nunc<sup>TM</sup>Lab-Tek Q5 Chambered Coverglass (Thermo Fisher Scientific, USA) were used. QuickFit 3.0[35] free software was employed for FCCS data analysis. To fit data, the global fitting with 1-2 components 3D normal diffusion model was applied. If a satisfactory fit was not obtained, a 1-component 3D normal diffusion model was applied only to the FCCS curve, and is specified in the caption of the table reporting the data. The confocal volume was determined using 25 nM Rhodamine 123 solution. Hydrodynamic radii were calculated applying the Stoke-Einstein equation:

$$D_c = \frac{k_B T}{6\pi\eta r_H}$$

where  $D_c$  is the diffusion coefficient derived from the FCCS fitting,  $k_B$  the Boltzmann constant,  $T$  the absolute temperature,  $\eta$  the viscosity and  $r_H$  the hydrodynamic radius. Further details on FCCS theory and experimental data are reported in the Supplementary Information.

### 2.2.3. FCCS and pH experiments

PAH/siRNA complexes were prepared in DNase/RNase-free distilled water pH 7.4 by mixing a fixed amount of PAH (1  $\mu$ M) with different amounts of siRNA (N/P = 40, 4, 2, and 1). After equilibration for 30 minutes at room temperature, measurements were performed. To acidify the medium, 1 M HCl was used, while 1 M NaOH was used to raise the pH. The solutions were equilibrated for a further 20 min prior to performing measurements. Data were recorded in 20 runs of 10 s each.

#### *2.2.4. Gel Retardation Assay*

The interaction between siRNA and polymer was investigated by electrophoresis on agarose gel. The agarose gel was prepared by dissolving 1 g of agarose powder in 100 mL Tris base, acetic acid and ethylenediaminetetraacetic acid (TEA buffer) containing 2  $\mu$ L GelRed® 10.000x (Biotium). Nanoparticles were prepared at different concentrations of PAH keeping the concentration of siRNA constant at 1  $\mu$ mol for N/P ratios = 0.1, 1, 2, 4 and 10. These samples were then vortexed and incubated at room temperature for 20 min. 20  $\mu$ L sample was mixed with 5  $\mu$ L gel loading buffer and loaded into the wells of the gel. Naked siRNA was used as a control and a dsRNA marker was used to control mobility of siRNA through the gel. Electrophoresis was performed at 80 V during 30 minutes and results were visualized under UV. The gel was imaged with a MULTIDOC-IT™ imaging System by UVP.

#### *2.2.5. Dynamic Light Scattering (DLS)*

Dynamic light scattering measurements were carried out with a  $\zeta$ -Sizer Malvern Instrument in backscattering mode. All studies were performed at a 173° scattering angle with

temperature controlled at 25 °C in 1 mL polystyrene cuvettes. Short time measurements were carried out for a total of 15 min, with 3 consecutive measurements for each sample.

#### *2.2.6. Transmission Electron Microscopy (TEM)*

Thirty minutes following PAH/siRNA nanoparticle assembly, 5 µL nanoparticles was transferred to ultrathin plasma coated carbon films and incubated for 1 min, then incubated with 3 µL of 20 mg/mL ammonium molybdate (negative stain) for 1 min and washed 3 times with degassed nanopure water. Imaging was carried out with a JEOL JEM 1010 transmission electron microscope operating at an acceleration voltage of 100 kV.

#### *2.2.7. Cell culture*

Lung adenocarcinoma cell line (A549) was cultured in RPMI 1640 medium supplemented with 10% (v:v) FBS and 1% (v:v) antibiotic solution (100 units/mL penicillin, 100 mg/mL streptomycin; P/S). Cells were maintained at 37 °C and 5% CO<sub>2</sub> in a humidified chamber. GFP-A549 cell lines were cultured with Ham's F-12K medium supplemented with 10% FBS, 1% P/S and blastidicin at 10 µg/mL.

#### *2.2.8. Viability Assay*

5000 cells per well were seeded in a 96-well plate and allowed to grow for 24 h. PAH/siRNA complexes at N/P ratios of 1, 2, 4 and 10 were formed by mixing appropriate amounts of polymer and  $5 \times 10^{-5}$  µmol siRNA in 50 µL RNase free water. Particles were stabilized for 30 min at room temperature and then added to the wells in a final volume of 100 µL. Cells were incubated with PAH/siRNA nanoparticles for 48 h and their viability

was measured by MTS assay. Briefly, after the 48 h of incubation, cells were washed with PBS and then 100  $\mu$ L of fresh medium was added. Then 20  $\mu$ L of CellTiter 96® AQueous One Solution Cell Proliferation Assay (MTS) from Promega was added to the wells and incubated for 2 h at 37 °C 5% CO<sub>2</sub>. The absorbance at 490 nm of the resulting solution was measured in a 96-well spectrophotometer microplate reader. Percentage cell mitochondrial activity was determined by the following formula: (Absorbance of treated cells/Absorbance of control cells) x 100. Data are represented as a mean $\pm$  standard deviation of 3 measurements.

#### *2.2.9. Cellular Uptake of PAH/R-siRNA nanoparticles.*

The cellular uptake of PAH/R-siRNA nanoparticles with different N/P ratios and at different times was quantified via flow cytometer. Cy-5 siRNA was complexed with different amount of non labelled PAH to get a final molar ratio of N/P = 2 and 4 respectively. Briefly, A549 cells were cultured on 24 well plates and exposed to nanoparticles with N/P 2 and N/P 4 for 3 and 24 hours at 5 % CO<sub>2</sub> and 37 °C. After incubation with PAH/R-siRNA nanoparticles cells were washed with PBS and trypsinized. Fluorescence of the cells was quantified and analyzed with a BD-FACs Canto II cytometer, (Becton Dickinson, USA). Measurements were performed in duplicate and approximately 10<sup>4</sup> events (cells)/ sample were analyzed. A549 cells not exposed to PANs were used as a control.

#### *2.2.10. FCCS experiments in living cells*

24 h before FCCS experiments, 4 x 10<sup>4</sup> A549 cells were seeded in an 8 well glass bottom plate with 500  $\mu$ L RPMI with 10% FBS and 1% P/S. Cells were washed 3 times with

phosphate buffer saline (PBS) and incubated with G-PAH/R-siRNA nanoparticles (N/P = 2) in 200  $\mu$ L RPMI complete medium. After 1 h of incubation, the non-internalized complexes were removed by washing 3 times with PBS. Experiments were conducted at time 0 using serum-free L15 medium to balance the CO<sub>2</sub> level. For follow-up experiments, washed cells were incubated at 37 °C with 500  $\mu$ L RPMI. After 24 h, cells were washed again twice and kept in L15 medium during the experiment. Data were recorded for at least 3 cells in different locations recording 20 runs of 10 s each.

#### *2.2.11. Confocal Laser Scanning Microscopy (CLSM)*

Cells prepared as for FCCS experiments were imaged with a Zeiss LSM 510 laser scanning microscope. CLSM imaging was performed by exciting at 405, 488, and 561 nm excitation laser lines, with a 63 $\times$  objective. Cells were observed at time 0 (just after incubation with nanoparticles), and after a further 24 h of incubation in RPMI complete medium.

Co-localization between the red (R-siRNA) and green (G-PAH) signals was determined using the JACoP plugin[36] of ImageJ. The threshold applied was determined by the Otsu Thresholding plugin.[37] The indexes considered for evaluating co-localization were the Pearson's coefficient,  $r$ , and the Mander's coefficients,  $M1$  and  $M2$ . Pearson's coefficient can assume values from 1 to -1, with 1 indicating total linear correlation between the intensities in two images and -1 no correlation.  $M1$  and  $M2$  are overlap coefficients based on the Pearson's correlation coefficient. They can vary from 0 to 1, and reflect the percentage co-localization between two images.  $M1$  is defined as the ratio of the "summed intensities of pixels from the green image for which the intensity in the red channel is above zero" to the "total intensity in the green channel".  $M2$  is defined the same way, but with respect to the red channel.

### *2.2.12. In vitro Transfection Assay*

Briefly,  $3 \times 10^4$  GFP-A549 cells were placed in a 24 well plate, in medium with 10% serum and 1% P/S the day before transfection. Before transfection experiments, cells were washed with medium containing 2% serum and then, 500  $\mu$ L fresh medium containing 2% serum was added to each well. The transfection was followed for 96 h. Cells were transfected with polyplexes made of PAH/siRNA and PEI/siRNA at different N/P ratios. The concentration of siRNA was fixed at 0.2  $\mu$ M in a final volume of 500  $\mu$ L per well. Lipofectamine RNAiMAX and PEI/siRNA nanoparticles were used as controls. Silencing efficacy was quantified by flow cytometry. Cells were washed with PBS, trypsinized, and fixed in 1% paraformaldehyde in PBS for 15 min at room temperature. Approximately  $1 \times 10^4$  events (cells) were analyzed for each sample while untreated GFP-expressing A549 cells were used as a positive control i.e. the fluorescence intensity value of the cells before silencing. The percentage of transfected cells was calculated as the number of GFP+ (positive) cells over the total population of analyzed cells. Experiments were performed with a BD FACSCalibur™ flow cytometer (BD Biosciences) and data were analyzed with the BD CELLQuest™ software (BD Biosciences). Experiments were repeated 3 times, n=3 and data are represented as a mean  $\pm$  standard deviation.

## **3. Results and Discussion**

### *3.1. Characterization of PAH/siRNA Nanoparticles*

The formation of nanoparticles was characterized by a gel retardation assay, DLS, and TEM measurements. To evaluate the ability of the polymers to complex with siRNA and

form nanoparticles, we determined the polymer nitrogen group/siRNA phosphate group molar ratio (N/P) at which siRNA became completely complexed. The gel retardation assay performed using PAH/siRNA at different ratios showed that siRNA is completely bound to PAH at  $N/P \geq 2$  (**Fig. 1B**).

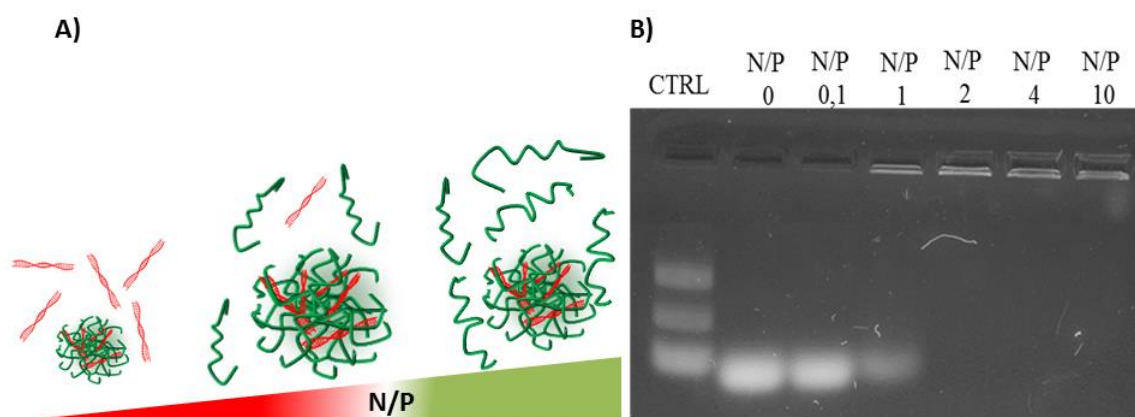


Fig.1. A) Formation of PAH/siRNA nanoparticles. G-PAH (green) and R-siRNA (red) were mixed at a defined stoichiometry determined from the ratio of positively charged amine groups from PAH and negatively charged phosphate groups from siRNA (N/P ratio). B) Gel retardation assay of PAH/siRNA nanoparticles prepared at different N/P molar ratios and incubated for 15 min at room temperature. Columns above each well indicate the PAH to siRNA molar ratio. siRNA is completely complexed to PAH at  $N/P \geq 2$ .

The hydrodynamic diameter measured by DLS of nanoparticles with  $N/P = 2$  is  $98 \pm 4$  nm with a polydispersity index (PDI) of  $0.23 \pm 0.03$  calculated by CUMULANT analysis (**Fig. 2A**). TEM images corroborate the data obtained by DLS (**Fig. 2B**); indeed, the size of nanoparticles for  $N/P = 2$  was calculated to be  $80 \pm 22$  nm.

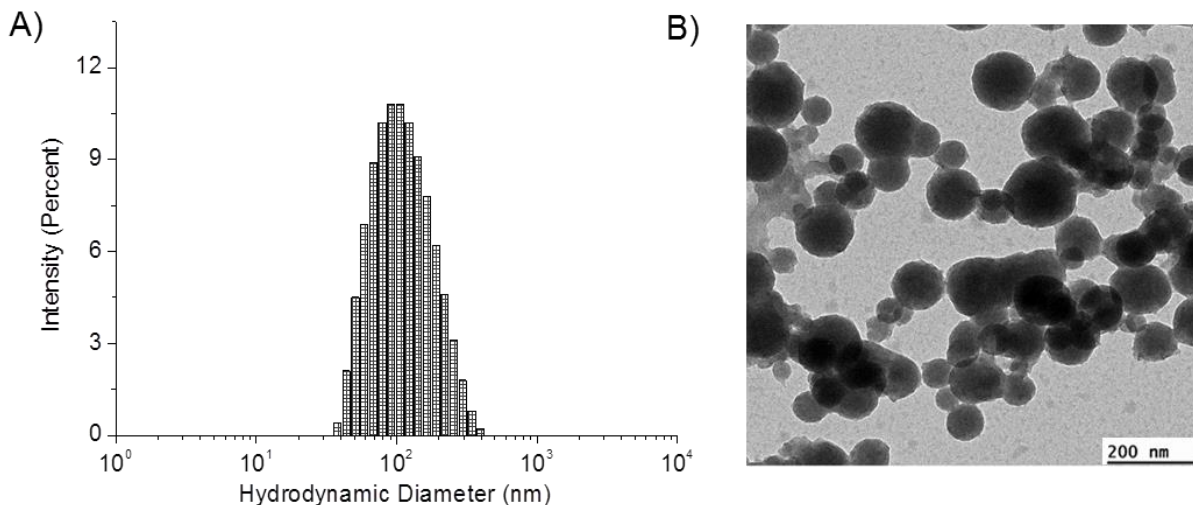


Fig. 2. A) DLS and B) TEM characterization of nanoparticle formation for PAH/siRNA complexes prepared at  $N/P = 2$ . Scale bar in B) corresponds to 200 nm. The hydrodynamic diameter determined from DLS ( $98 \pm 4$  nm) is corroborated by the diameter determined from TEM images ( $80 \pm 22$  nm).

FCS and FCCS experiments were carried out using fluorescently labelled green rhodamine PAH (G-PAH) and Cy5-siRNA (R-siRNA). Nanoparticles were formed at various PAH/siRNA molar ratios, leading to self-assembled nanoparticles of different composition, size, and stability.

**Fig. 3** reports cross-correlation curves from FCCS for PAH/siRNA nanoparticles at  $N/P = 2$ . The correlograms corresponding to the FCS autocorrelation functions from red and green channels resulting from the fluorescence fluctuations of R-siRNA and G-PAH, respectively, are shown in Fig. S1. For the relative cross-correlations  $FCCS/ACF\_R\text{-siRNA}$  and  $FCCS/ACF\_G\text{-PAH}$ , the normalized cross-correlation amplitude at time zero can be used with some simplifications to express the fraction of siRNA and PAH in the nanoparticles and can assume values from 0 to 1, with 0 indicating no association of the



two species and 1 indicating complete association. The amplitude of the cross-correlation at time zero is directly related to the amount of the two labeled species, R-siRNA and G-PAH, present in the confocal volume.[38] Nanoparticles were prepared with different N/P ratios: with an excess of amines to phosphates ( $N/P > 1$ ), with approximately equal amounts of amines and phosphates ( $N/P \sim 1$ ), or with an excess of phosphates to amines ( $N/P < 1$ ). The composition of the complexes is different in each case as implied by the different relative cross-correlations observed (**Fig. S1**). When there was a slight excess of phosphates to amines such as  $N/P = 0.6$ , small complexes are formed with a hydrodynamic diameter ( $R_H$ ) of  $7.5 \pm 0.1$  nm. In complexes with  $N/P = 1.2$  all the siRNA is associated in nanoparticles with a hydrodynamic diameter,  $R_H = 22.6 \pm 0.2$  nm, and there is an excess of free PAH (FCCS/ACF\_R-siRNA = 1 and FCCS/ACF\_G-PAH = 0.1 (**Fig. S1, Table S1**). The free PAH diffuses with a diffusion coefficient  $R_c = 48.5 \pm 6.1 \mu\text{m}^2/\text{s}$ , which is about 10 times faster than the double-labeled species, which has a  $R_c = 4.75 \pm 0.05 \mu\text{m}^2/\text{s}$ . For  $N/P = 2.4$  the complexation of PAH and siRNA was confirmed with FCCS (**Fig. 3A**). These nanoparticles show a diffusion coefficient  $R_c = 2.6 \pm 0.05 \mu\text{m}^2/\text{s}$  and normalized cross-correlations of 0.2 for FCCS/ACF\_R-siRNA and 0.4 for FCCS/ACF\_G-PAH, indicating that the nanoparticles are in equilibrium with free siRNA ( $R_c = 22.55 \pm 2.05 \mu\text{m}^2/\text{s}$ ) and PAH molecules (**Table S1**). At  $N/P = 2.4$  the nanoparticles have an hydrodynamic diameter  $R_H = 41.3 \pm 0.8$  nm, about twice as large as that observed for nanoparticles with  $N/P = 1.2$ . The same trend was confirmed by DLS (data not shown). N/P ratios with an excess of amines to phosphate such as  $N/P = 4$  and  $N/P = 50$ , did not result in stable polymer complexes (**Figure S1, Table S1**).

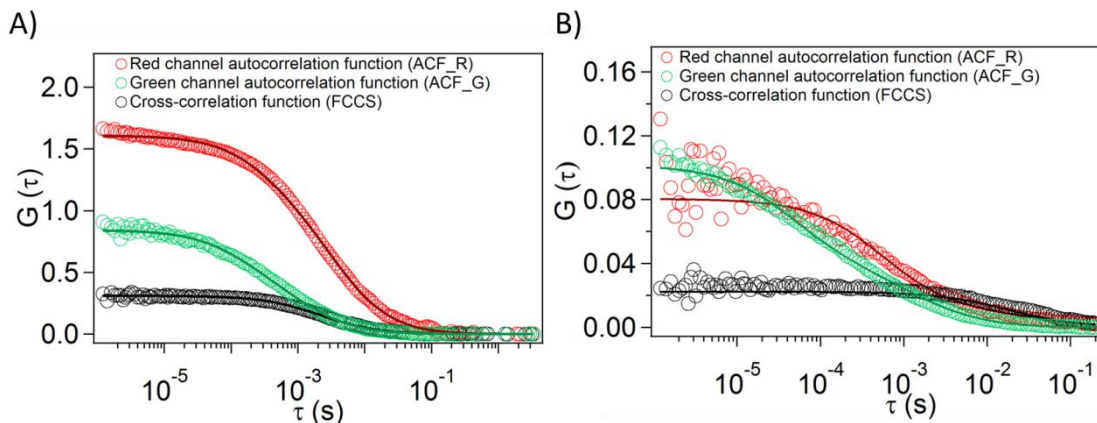


**Fig. 3.** FCCS correlation functions of PAH/siRNA complexes at  $N/P = 2$ . A) Nanoparticles were formed in RNase free water equilibrated at room temperature for 30 minutes before the measurements. B) Nanoparticles formed by mixing G-PAH and R-siRNA at  $N/P = 2$  were diluted with RPMI complete medium. The samples were equilibrated for 30 minutes and measured up to 1 h after equilibration. Data are reported in **Table S2** together with those from single molecules tested in RPMI (**Fig. S2**). Red circles indicate the autocorrelation function in the red channel (ACF\_R  $\lambda_{ex} = 633$  nm) of Cy5-siRNA, and green circles indicate the autocorrelation function in the green channel (ACF\_G  $\lambda_{ex} = 488$  nm) of PAH labelled with rhodamine green. Black circles show the cross-correlation function (FCCS). Solid lines are the fittings.

### 3.2. Stability studies of PAH/siRNA nanoparticles

The stability of PAH/siRNA nanoparticles was tested in RPMI 1640 complete medium, commonly used for *in vitro* experiments (with 10% fetal bovine serum, and 1% penicillin/streptomycin). The stability of the nanoparticles was evaluated at three different ratios:  $N/P < 2$ ,  $N/P = 2$  and  $N/P > 2$ . The nanoparticles were added to the RPMI full media and left to equilibrate for 30 minutes at room temperature. Measurements were performed

up to 1 h after equilibration. Nanoparticles with  $N/P = 2$  retain cross-correlation (**Fig. 3B**). However, the size of the nanoparticles approximately doubles ( $D_C = 2.1 \pm 0.1 \mu\text{m}^2/\text{s}$  and  $D_H = 204.4 \pm 9.8 \text{ nm}$ ), while the relative cross-correlations FCCS/ACF\_G-PAH and FCCS/ACF\_R-siRNA remain almost unaltered, both with values of 0.3 (**Table S2**), indicating that the complexes are stable in medium. Nanoparticles with  $N/P > 2$  and  $N/P < 2$  form aggregates with diffusion times exceeding the technique limit (**Fig. S2C and S2D**, and **Table S2**).

This difference may be attributed to the presence of proteins forming a protein corona or the association of several nanoparticles through interaction with proteins.[39,40] It could also result from conformational changes in PAH molecules[41] due to the increased ionic strength ( $\sim 150 \text{ mM NaCl}$ ); or to the presence of phosphate ions in the RPMI medium interacting with PAH, which may lead to nanoparticle reorganization.[32] There is  $\sim 5 \text{ mM}$  sodium phosphate dibasic in RPMI. Phosphate ions could easily interact with PAH amine groups and cause nanoparticle reassembly by replacing the phosphate ions of the siRNAs. However, such colloidal instability is not observed for nanoparticles with  $N/P = 2$ , meaning that they have a more stable structure. When we consider PAH and siRNA individually, G-PAH was affected more by the change of environment ( $D_c = 12.9 \pm 0.6 \mu\text{m}^2/\text{s}$  compared to  $D_C = 97.1 \pm 12.2 \mu\text{m}^2/\text{s}$  in water) while the R-siRNA was not altered ( $D_C = 43.0 \pm 2.6 \mu\text{m}^2/\text{s}$  compared to  $D_C = 45.1 \pm 4.1 \mu\text{m}^2/\text{s}$  in water). This result is expected as PAH is a flexible polyelectrolyte, which can easily change conformation in response to changes in ionic strength and pH (**Fig. S3 and Table S2**).[42]

The stability of PAH/siRNA nanoparticles at biologically relevant pHs was studied to assess their potential for intracellular delivery of siRNA. An ideal vector should be stable during circulation, i.e. at pH 7.4, and only degrade in the endosomal compartments after

cellular uptake at a pH close to 5.[11,43] FCCS experiments were performed at pH 7.4, 6, 5, 2 and 8. Lowering of the pH caused a gradual rearrangement of the complexes that ended in nanoparticle dissociation (**Fig. 4** and **Table S3**). The amplitudes of both the autocorrelation curves of PAH and siRNA, and the cross-correlation curves decreased progressively when the pH was decreased from 7.4 to 5 and finally to 2 (**Fig. 4**). This trend for the autocorrelation curves is associated with an increase in the number of single-labeled species in the confocal volume, likely due to nanoparticle dissociation. This hypothesis is supported by the amplitude decrease in the cross-correlation curves, which is directly related to the number of complexes displaying two labels. The nanoparticles progressively decrease in size with decreasing pH (**Fig. 4**). The hydrodynamic diameter at pH 7.4 is  $82.6 \pm 1.6$  nm, at pH 5 is  $57.2 \pm 2.2$  nm and at pH 2 is  $22.2 \pm 0.4$  nm. The corresponding diffusion coefficients are  $D_c = 5.2 \pm 0.1 \mu\text{m}^2/\text{s}$ ,  $7.5 \pm 0.3 \mu\text{m}^2/\text{s}$ ,  $19.3 \pm 0.3 \mu\text{m}^2/\text{s}$  respectively. The sudden increase in the pH up to 8 from acid pHs results in an increase of the cross-correlation amplitude (**Fig. 4C**). The autocorrelation functions of the siRNA and PAH also increased (**Fig. 4A** and **4B**), indicating less free diffusing fluorescent species and more association between PAH and siRNAs for nanoparticle formation with a slightly larger hydrodynamic diameter than the starting nanoparticles at pH 7.4, ( $107.4 \pm 2.6$  nm vs.  $82.6 \pm 0.4$  nm). Conversely, the diffusion times of the single species of G-PAH and R-siRNA were not affected by the pH change (**Figure S3**). DLS measurements confirmed these trends (data not shown). These experiments show that the nanoparticles have a dynamic nature, which is highly sensitive to pH. Changes in pH can cause re-assembly to produce nanoparticles with different hydrodynamic sizes. At acid pH we can assume that the phosphate groups of the siRNAs lose their charge, which affects their interaction with PAH, resulting in nanoparticle disassembly. At moderate basic pH, amines in PAH

probably retain enough charges to remain assembled with siRNA, but the electrostatic repulsion between PAH chains of the same charge decreases, which allows the nanoparticles to grow in size. Switching from acid to basic pH results in the reassembly of nanoparticles from single components. However, the most important message from these experiments is that the nanoparticles are stable at neutral pH and should therefore be stable during circulation. The nanoparticles start to degrade at moderately acidic pH, suggesting a priori that the siRNAs will be released only when they are inside endosomes. To prove this, we conducted intracellular FCCS and CLSM experiments. Since nanoparticles with  $N/P = 2$  are more stable in RPMI, these nanoparticles were chosen for further FCCS experiments at different pH and intracellularly.

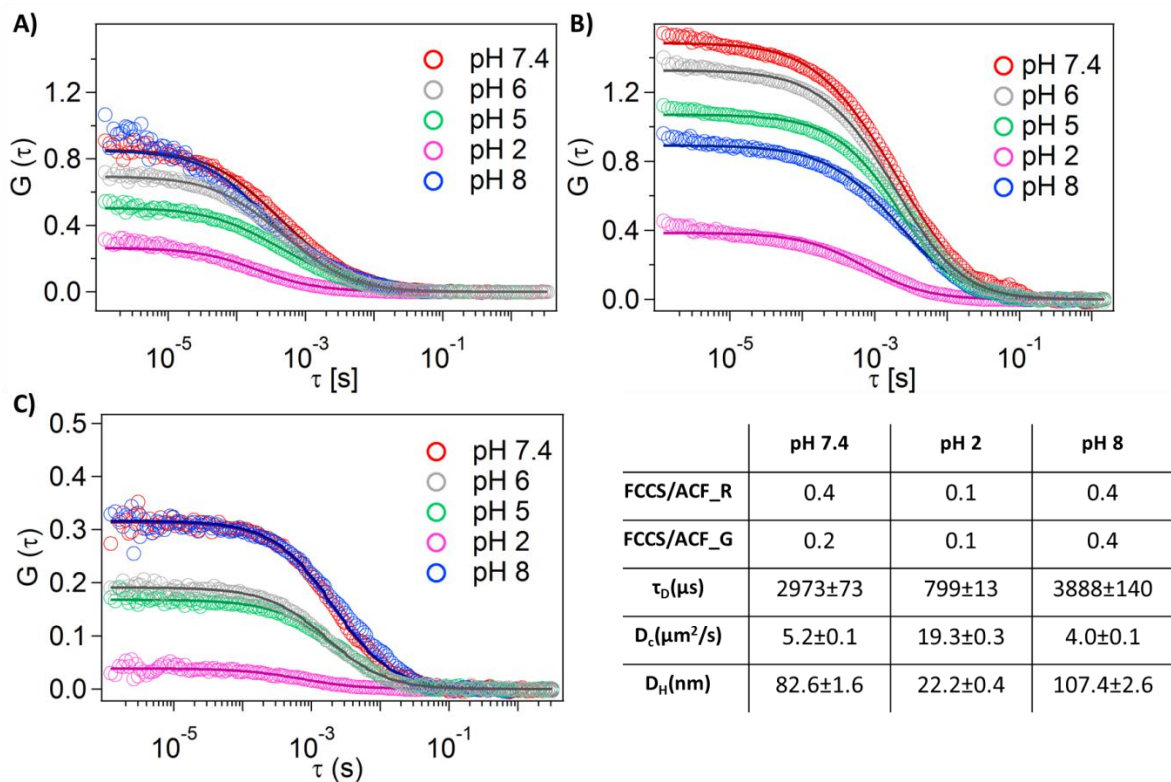


**Fig. 4.** Autocorrelation functions ACF\_R-siRNA (A) and ACF\_G-PAH (B) and cross-correlation (C) of PAH/siRNA nanoparticles at different pH. PAH/siRNA nanoparticles (N/P = 2) were characterized at neutral pH (pH 7.4, red circles), pH 6 (grey circles), pH 5 (green circles), pH 2 (pink circles) and after addition of NaOH 1 M to bring the pH from 2 to 8 (pH 8, blue circles). Solid lines correspond to the fittings. The table on the right reports data from the displayed fitting at meaningful pH values. Full data are reported in **Table S3**.

### 3.3. Intracellular trafficking of PAH/siRNA nanoparticles

#### 3.3.1. Cell viability

Before studying cell fate and siRNA transfection, cell viability of PAH/siRNA nanoparticles was evaluated in the A549 cell line up to 48 h employing a N/P molar ratio in the range of 1 – 10, that corresponds to a PAH concentration of  $10^{-3}$  –  $10^{-1}$  mg/mL, or 0.01 – 1.1 mM in terms of PAH monomers (monomer molecular weight: 94). Cell viability assays show between 80 and 100% viability for N/P ratios up to 4 but when reaching an N/P ratio of 10 viability decreases to less than a 10% (**Fig. 5**). This result means that up to N/P = 4, nanoparticles can be considered non-cytotoxic. Therefore values of  $N/P \leq 4$  were used for the following in vitro experiments.

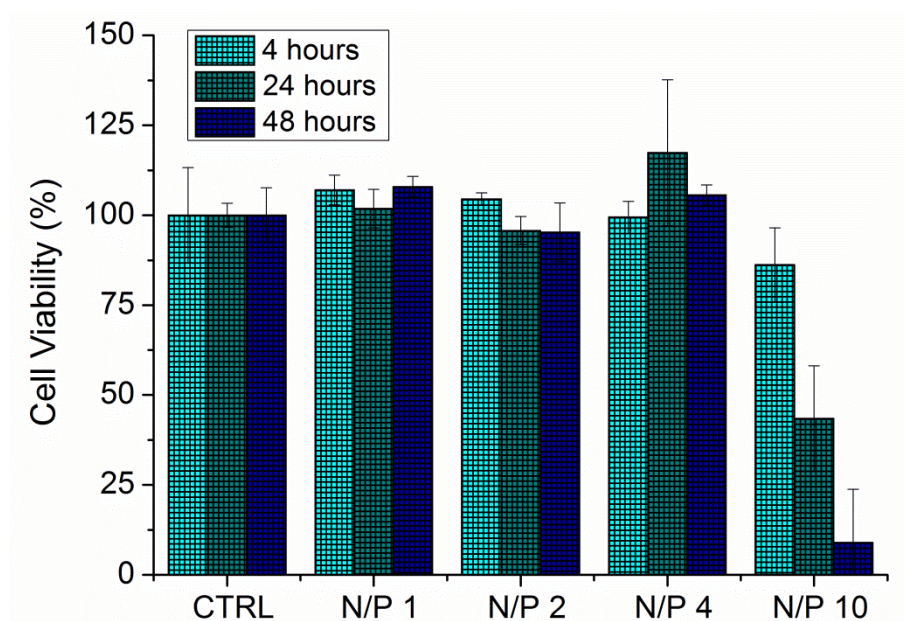


**Fig. 5:** Percentage of cell viability of A549 cells after 4, 24 and 48 h exposure to PAH/siRNA nanoparticles at different N/P ratios. Error bars represent the standard deviation of duplicate samples.

#### 3.3.2. Cellular uptake

Cellular internalization of PAH/Cy5-siRNA was quantified via flow cytometry at two time points, 3 and 24 h. Fluorescent siRNA was used to quantify the cellular uptake of PAH/siRNA nanoparticles at two different ratios, N/P = 2 and 4. The fluorescence intensity increased as the incubation time of the nanoparticles increased (**Fig. 6**). No significant differences in uptake are observed for the two N/P ratios within the time frame of the measurements.

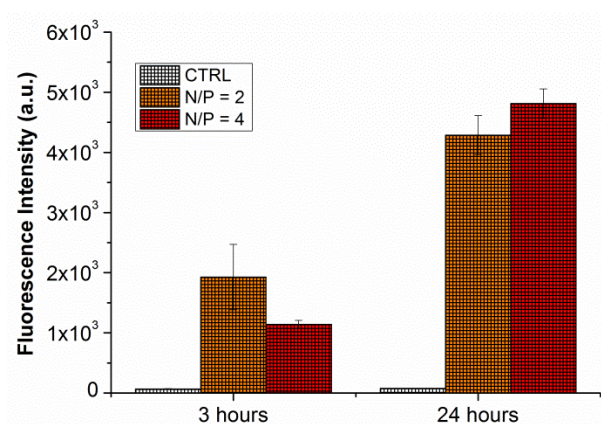


**Fig. 6.** Mean Fluorescence intensity (a.u.) measured by flow cytometry, of A549 cells at 3 and 24 hours after internalization of PAH/R-siRNA nanoparticles at N/P = 2 and N/P = 4. Cells not exposed to nanoparticles were used as a control. Cell cultures were always exposed to the same concentration of R-siRNA used in the transfection experiments and different amount of PAH. The error bars represent the standard deviation of duplicate samples.

### 3.3.3. Intracellular trafficking in live cells

The intracellular trafficking of internalized PAH/siRNA nanoparticles at N/P = 2 was followed by FCCS and CLSM after 1 h and after 24 h of incubation in controlled conditions. Data were also collected at intermediate time-points, including 6 h and 12 h after incubation, but did not show any significant difference with respect to time zero and



are not shown here. FCCS measurements were taken at different locations inside the cells. Each measurement involved 20 repetitions of 10 seconds each. Initial bleaching was frequent especially after one hour of incubation. When bleaching happened in one of the three channels or in all of them, the first 20 seconds were reported separately from the rest of the averaged data (solid and empty dots in **Fig. 7** respectively). After 1 h of incubation, PAH and siRNA were associated with big cell machineries and/or fixed structures that prevented their free diffusion in cell compartments.[44] This observation is supported by the detection of many events of fluorescence bleaching (**Fig. 7**). Since the large and slow-diffusing complexes remain longer in the confocal volume, they are irradiated longer and experience bleaching. Once these large aggregates are bleached, the fluorescence intensities in the confocal volume are significantly lower, making it possible to detect fluorescence fluctuations from fast-diffusing species.[45] Only a small part of these “fast” species showed cross-correlation (7% of the total of the measures). A total of 79% of the fast-diffusing species were G-PAH (**Fig. S4**). After 24 h, bleaching events were significantly reduced and individual PAH and siRNAs are detected (**Fig. 7**). This observation suggests a decrease in co-localization of siRNAs and PAH. Interestingly, at this time-point, 83% of the individually diffusing species is R-siRNA molecules. The diffusion times of these molecules varied significantly from 300  $\mu$ s to  $10^4$   $\mu$ s (**Fig. S5** and **Table S4**). The wide distribution of diffusion times can be ascribed to the R-siRNAs interacting with several cellular proteins or machineries, or experiencing environments of different viscosity inside the cells.[46] It is plausible that R-siRNAs showing diffusion times of  $\sim 300$   $\mu$ s might be localized in the cytoplasm where the viscosity is similar to that of RPMI cell medium (see **Table S2**).[44]

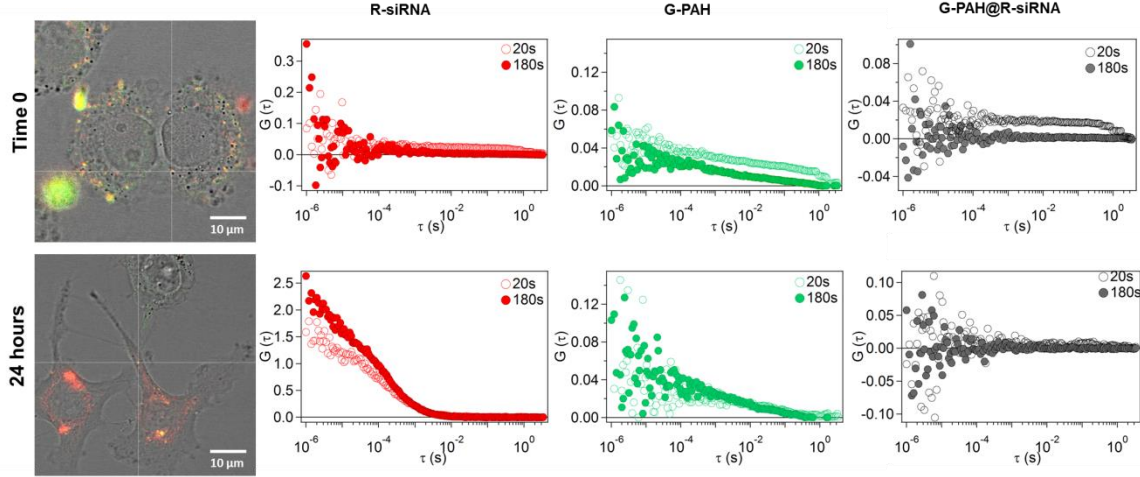


**Fig. 7.** Representative cross-correlation experiment in live cells. A549 cells were imaged in transmission mode and cross-correlation was measured at specific locations inside the cell (white cross). Cells were incubated with the nanoparticles ( $N/P = 2$ ) in RPMI complete medium. The cells were imaged just after incubation with the nanoparticles (Time 0), and after incubation for a further 24 h in complete medium under controlled conditions (37 °C and 5%  $CO_2$ ). The autocorrelation function in the red channel (ACF\_R  $\lambda_{ex} = 633\text{nm}$ , red markers) is associated with R-siRNA, and the autocorrelation function in the green channel (ACF\_G  $\lambda_{ex} = 488\text{nm}$ , green markers) is associated with G-PAH. The cross-correlation curve is represented by black markers (FCCS) and is associated with PAH/siRNA nanoparticles. Each location was measured in 20 runs of 10 s each. Average curves are reported after 20 s (runs 1-2) and 180 s (runs 3-20).

Co-localization experiments were performed at different time points to corroborate our FCCS findings confirming a significant decrease in the co-localization between the red and green channels after 24 h (**Fig. 8**). Both Pearson's coefficient,  $r$ , and Mander's coefficients,  $M1$  and  $M2$ , decrease by about 50% after 24 h. While Pearson's coefficient indicates the degree of linear correlation between red and green channels, Mander's coefficients give the percentage of co-localization. The decrease in co-localization corroborates FCCS results and is due to the intracellular disassembly of the PAH/siRNA complexes. The fate of the nanoparticles inside cells is sketched in **Scheme 1**. After cellular uptake, complexes are translocated in endosomal compartments displaying acidic pH that favours their spontaneous dissociation and the diffusion of siRNA in the cytoplasm ().

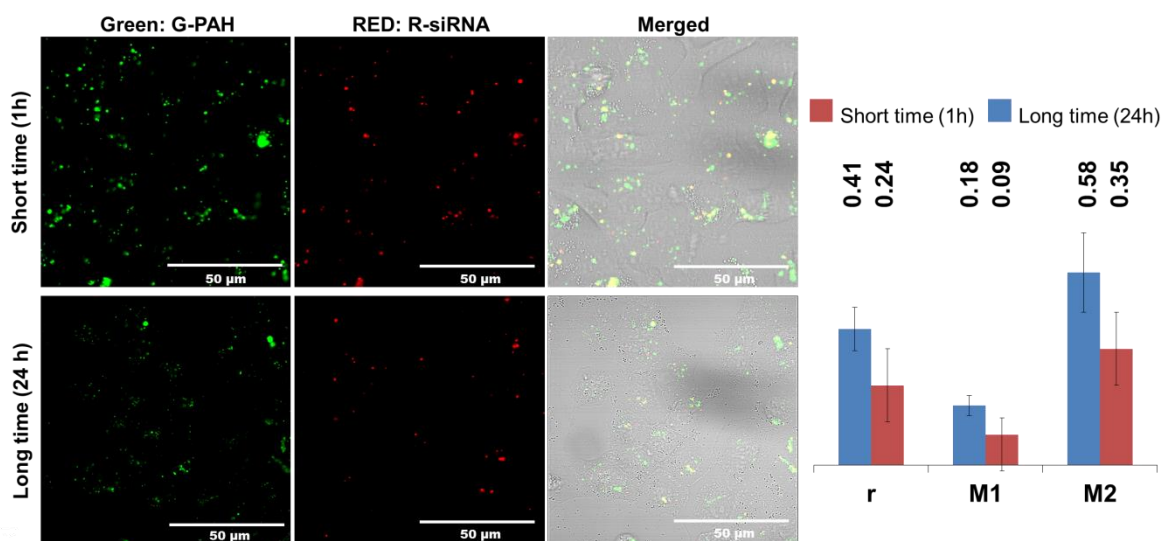
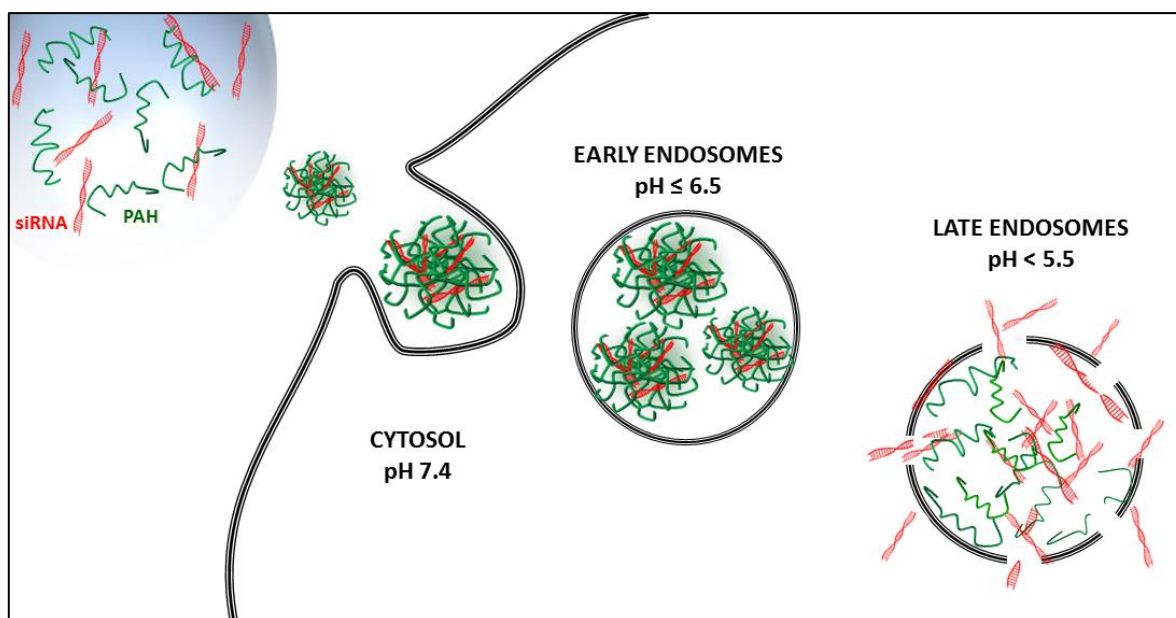


**Fig. 8.** CLSM micrographs showing co-localization between red (R-siRNA) and green (G-PAH) channels. Cells not exposed to nanoparticles (CTRL) and naked siRNA were used as controls. Images were taken after incubating cells with nanoparticles for 1 h and 24 h. Confocal micrographs collected in different areas of the samples were analyzed using the

JACoP plugin for ImageJ. Co-localization by time is demonstrated by Pearson's coefficient (r) and Mander's coefficients (M1 and M2) reported in the histogram.



**Scheme 1.** Uptake and intracellular fate of PAH/siRNA nanoparticles. The scheme describes the uptake and degradation of the nanoparticles into endosomes. The degradation of the nanoparticles is shown by the presence of free PAH (red) and siRNA (green) at low endosomal pH. The translocation of the siRNAs from the endosomes to the cytoplasm is indicated by the presence of free siRNA outside endosomal compartments.

#### *3.3.4. Silencing efficiency of PAH/siRNA nanoparticles*

The GFP-A549 cell line was used for silencing experiments because it has a stable expression of GFP that can be knocked down by the delivery of specific siRNAs. Flow cytometry analysis was carried out to quantify the efficacy of siRNA delivered by PAH/siRNA nanoparticles compared with PEI/siRNA as a control. PEI is the most

frequently used polycation for gene delivery. Flow cytometry allows evaluation of the efficacy of GFP silencing by measuring the fluorescence intensity per cell after transfection (**Fig. 9**). Transfections were performed using different N/P ratios. The efficacy of PAH/siRNA for silencing was compared with siRNA delivered by PEI, which is known to effectively silence GFP.[47] The expression level of GFP in GFP-A549 cells, decreased by ~55% in cells treated with N/P = 2 compared to untreated cells. For N/P = 4, the fluorescence intensity of the cells decreased by up to 75%, indicating good silencing efficiency of PAH/siRNA nanoparticles. When naked-siRNA was used as a control, no inhibition of GFP expression was observed.

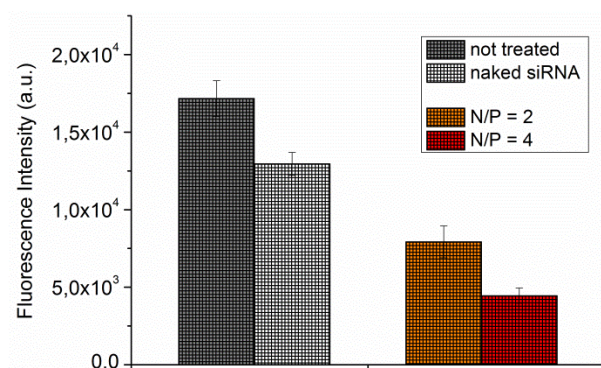


**Fig. 9.** Mean Fluorescence intensity (a.u.) of GFP-A549 cells treated with PAH/siRNA at N/P = 2 and N/P = 4. The silencing efficacy of PAH/siRNA at N/P = 2 (orange bar) and N/P = 4 (red bar) are reported. As a control, data from GFP-A549 cells treated with naked siRNA (white bar) and from untreated cells (grey bar) are reported. All samples were treated with the same concentration of siRNA. Error bars represent the standard deviation of duplicate samples.

Results from GFP silencing show that the silencing by PAH/siRNA is effective at low N/P values at which PEI/siRNA nanoparticles do not show effective silencing. For  $N/P = 2$ , silencing by PEI/siRNAs is not more than a 10% (**Fig. S6**). The higher efficacy shown by PAH/siRNA could probably be attributed to the better complexation by PAH, a linear polymer with only primary amines, to siRNA with a relatively small excess of amine groups to phosphate. PAH/siRNA nanoparticles have the advantage of being highly stable in neutral environments and disassembling at endosomal pH 5.5, which favors the liberation of the siRNAs. At this pH, PAH molecules protonate and can induce endosomal breakage, which can also trigger the translocation of siRNAs into cytosol.

#### **4. Conclusion**

We studied the complexation of PAH and siRNAs, and nanoparticle formation by gel retardation, TEM, DLS and FCS/FCCS. By FCCS, we obtained detailed information on the complexation of PAH and siRNA, which showed that the complexation, formation and stability of PAH/siRNA nanoparticles is dependent on the ratio of charged amines in PAH to charged phosphate groups in siRNA (N/P), and on environmental conditions such as pH, and the presence of phosphates and/or proteins in media. With FCCS we showed that the most stable nanoparticles are formed by complexation of PAH and siRNA in water with  $N/P = 2$ . PAH/siRNA nanoparticle reorganization is triggered by variations in pH. The nanoparticles disassemble in moderately acid pH similar to that found in the endosomal environment, around 5.5. PAH/siRNA nanoparticles have a dynamic nature, being able to reassemble from molecular components into nanoparticles when increasing the pH from acid to moderately basic pH. Intracellular studies by FCCS and FCS revealed that at early

stages, PAH/siRNA nanoparticles rearrange inside cells forming large aggregates, probably by interacting with cell structures and proteins, but later they disassemble liberating the siRNAs. Cytosol translocation of siRNAs is confirmed by CLSM imaging. Our experiments demonstrate a time-scale for the endocytic release of siRNAs from the nanoparticles: association between PAH and siRNA in the form of slow-diffusing species could be detected for up to 12 h (early and late endosomes). After 24 h, a significant decrease in PAH and siRNA co-localization was observed, and free siRNA (characterized by faster diffusion times), could be detected, indicating an effective endosomal escape in the cytoplasm. The combined use of FCS and FCCS enabled us to analyze the reorganization and compositional changes of nanoparticles in different environments, including in cell media and inside cells, and to demonstrate nanoparticle degradation intracellularly. Moreover, FCS/FCCS allowed us to trace the molecular components PAH and siRNA individually both in bulk and intracellularly, which cannot be assessed with other experimental techniques.

PAH/siRNA nanoparticles with  $N/P = 4$  showed no cellular toxicity and result in the silencing of GFP expression in cells overexpressing this protein to approximately 50%; cells treated with PEI/siRNA nanoparticles at the same N/P ratio only resulted in a 10% decrease in GFP expression at most. These results hint at the potential advantages of PAH/siRNA complexes for silencing therapies at low N/P ratios where particles are not cytotoxic.

Our work also brings insight into the translocation process of the nanoparticles and the mechanism by which the siRNAs are delivered in the cytosol, which is fundamental for designing effective delivery systems for nucleic acids based on charged polymers.

## ASSOCIATED CONTENT

### Supporting Materials

Theory of FCS and FCCS (PDF); FCCS characterization of PAH/siRNA nanoparticles in RNase free water (PDF); FCCS characterization of PAH/siRNA nanoparticles in RPMI (PDF); Stability of siRNA/PAH nanoparticles at different pH (PDF); FCCS in cells (PDF)

## AUTHOR INFORMATION

### Corresponding Authors

\*Sergio E. Moya: [smoya@cicbiomagune.es](mailto:smoya@cicbiomagune.es)

Patrizia Andreozzi: [pandreozi@cicbiomagune.es](mailto:pandreozi@cicbiomagune.es)

## ACKNOWLEDGMENTS

The authors thank the MAT2017-88752-R2017 Retos project from the Spanish Ministry of Economics. This work was performed under the Maria de Maeztu Units of Excellence Program from the Spanish State Research Agency – Grant No. MDM-2017-0720.

## ABBREVIATIONS

CLSM, confocal laser scanning microscopy; DLS, dynamic light scattering; FCCS, fluorescence cross-correlation spectroscopy; FCS, fluorescence correlation spectroscopy; GFP, green fluorescent protein; G-PAH, green rhodamine labeled poly(allylamine hydrochloride); N/P, nitrogen to phosphate molar ratio; PAH, poly(allylamine hydrochloride); PEI, polyethylenimine; R-siRNA, Cy5 labeled silencing RNA; TEM, transmission electron microscopy.



## REFERENCES

- [1] K.A. Whitehead, R. Langer, D.G. Anderson, Knocking down barriers: Advances in siRNA delivery, *Nat. Rev. Drug Discov.* 8 (2009) 129–138. doi:10.1038/nrd2742.
- [2] A. Wittrup, J. Lieberman, Knocking down disease: A progress report on siRNA therapeutics, *Nat. Rev. Genet.* 16 (2015) 543–552. doi:10.1038/nrg3978.
- [3] H.J. Kim, A. Kim, K. Miyata, K. Kataoka, Recent progress in development of siRNA delivery vehicles for cancer therapy, *Adv. Drug Deliv. Rev.* 104 (2016) 61–77. doi:10.1016/j.addr.2016.06.011.
- [4] Y.K. Oh, T.G. Park, siRNA delivery systems for cancer treatment, *Adv. Drug Deliv. Rev.* 61 (2009) 850–862. doi:10.1016/j.addr.2009.04.018.
- [5] Y. Lei, L. Tang, Y. Xie, Y. Xianyu, L. Zhang, P. Wang, Y. Hamada, K. Jiang, W. Zheng, X. Jiang, Gold nanoclusters-assisted delivery of NGF siRNA for effective treatment of pancreatic cancer, *Nat. Commun.* 8 (2017) 1–15. doi:10.1038/ncomms15130.
- [6] H. Lee, I.K. Kim, T.G. Park, Intracellular trafficking and unpacking of sirna/quantum dot-pei complexes modified with and without cell penetrating peptide: Confocal and flow cytometric fret analysis, *Bioconjug. Chem.* 21 (2010) 289–295. doi:10.1021/bc900342p.
- [7] D. V. Morrissey, J.A. Lockridge, L. Shaw, K. Blanchard, K. Jensen, W. Breen, K. Hartsough, L. Machemer, S. Radka, V. Jadhav, N. Vaish, S. Zinnen, C. Vargeese, K. Bowman, C.S. Shaffer, L.B. Jeffs, A. Judge, I. MacLachlan, B. Polisky, Potent and persistent in vivo anti-HBV activity of chemically modified siRNAs, *Nat.*

Biotechnol. 23 (2005) 1002–1007. doi:10.1038/nbt1122.

- [8] J. Gu, K. Al-Bayati, E.A. Ho, Development of antibody-modified chitosan nanoparticles for the targeted delivery of siRNA across the blood-brain barrier as a strategy for inhibiting HIV replication in astrocytes, *Drug Deliv. Transl. Res.* 7 (2017) 497–506. doi:10.1007/s13346-017-0368-5.
- [9] H. Kuwahara, K. Nishina, K. Yoshida, T. Nishina, M. Yamamoto, Y. Saito, W. Piao, M. Yoshida, H. Mizusawa, T. Yokota, Efficient in vivo delivery of siRNA into brain capillary endothelial cells along with endogenous lipoprotein, *Mol. Ther.* 19 (2011) 2213–2221. doi:10.1038/mt.2011.186.
- [10] M. Zheng, W. Tao, Y. Zou, O.C. Farokhzad, B. Shi, Nanotechnology-Based Strategies for siRNA Brain Delivery for Disease Therapy, *Trends Biotechnol.* 36 (2018) 562–575. doi:10.1016/j.tibtech.2018.01.006.
- [11] J. Wang, Z. Lu, M.G. Wientjes, J.L.-S. Au, Delivery of siRNA Therapeutics: Barriers and Carriers, *AAPS J.* 12 (2010) 492–503. doi:10.1208/s12248-010-9210-4.
- [12] C.E. Thomas, A. Ehrhardt, M.A. Kay, Progress and problems with the use of viral vectors for gene therapy, *Nat. Rev. Genet.* 4 (2003) 346–358. doi:10.1038/nrg1066.
- [13] M. Dominska, D.M. Dykxhoorn, Breaking down the barriers: siRNA delivery and endosome escape, *J. Cell Sci.* 123 (2010) 1183–1189. doi:10.1242/jcs.066399.
- [14] D.J. Gary, N. Puri, Y.Y. Won, Polymer-based siRNA delivery: Perspectives on the fundamental and phenomenological distinctions from polymer-based DNA delivery, *J. Control. Release.* 121 (2007) 64–73. doi:10.1016/j.jconrel.2007.05.021.

- [15] B. Khurana, A.K. Goyal, A. Budhiraja, D. Arora, S.P. Vyas, siRNA Delivery Using Nanocarriers - An Efficient Tool for Gene Silencing, *Curr. Gene Ther.* 10 (2010) 139–155. doi:10.2174/156652310791111010.
- [16] P. Vader, L. J. van der Aa, G. Storm, R. M. Schiffelers, J. F.J. Engbersen, Polymeric Carrier Systems for siRNA Delivery, *Curr. Top. Med. Chem.* 12 (2012) 108–119. doi:10.2174/156802612798919123.
- [17] L. Desigaux, M. Sainlos, O. Lambert, R. Chevre, E. Letrou-Bonneval, J.-P. Vigneron, P. Lehn, J.-M. Lehn, B. Pitard, Self-assembled lamellar complexes of siRNA with lipidic aminoglycoside derivatives promote efficient siRNA delivery and interference, *Proc. Natl. Acad. Sci.* 104 (2007) 16534–16539. doi:10.1073/pnas.0707431104.
- [18] H. Takemoto, N. Nishiyama, Functional polymer-based siRNA delivery carrier that recognizes site-specific biosignals, *J. Control. Release.* 267 (2017) 90–99. doi:10.1016/j.jconrel.2017.09.005.
- [19] R. Macháň, T. Wohland, Recent applications of fluorescence correlation spectroscopy in live systems, *FEBS Lett.* 588 (2014) 3571–3584. doi:10.1016/j.febslet.2014.03.056.
- [20] D. Wöll, Fluorescence correlation spectroscopy in polymer science, *RSC Adv.* 4 (2014) 2447–2465. doi:10.1039/C3RA44909B.
- [21] K. Bacia, P. Schwille, Practical guidelines for dual-color fluorescence cross-correlation spectroscopy, *Nat. Protoc.* 2 (2007) 2842–2856. doi:10.1038/nprot.2007.410.

- [22] P. Schwille, F.J. Meyer-Almes, R. Rigler, Dual-color fluorescence cross-correlation spectroscopy for multicomponent diffusional analysis in solution, *Biophys. J.* 72 (1997) 1878–1886. doi:10.1016/S0006-3495(97)78833-7.
- [23] M. Baudendistel, G. Müller, W. Waldeck, P. Angel, J. Langowski, Two-hybrid fluorescence cross-correlation spectroscopy detects protein-protein interactions in vivo, *ChemPhysChem.* 6 (2005) 984–990. doi:10.1002/cphc.200400639.
- [24] D.R. Larson, J.A. Gosse, D.A. Holowka, B.A. Baird, W.W. Webb, Temporally resolved interactions between antigen-stimulated IgE receptors and Lyn kinase on living cells, *J. Cell Biol.* 171 (2005) 527–536. doi:10.1083/jcb.200503110.
- [25] T. Kohl, E. Haustein, P. Schwille, Determining protease activity in vivo by fluorescence cross-correlation analysis, *Biophys. J.* 89 (2005) 2770–2782. doi:10.1529/biophysj.105.061127.
- [26] M. Tiwari, S. Oasa, J. Yamamoto, S. Mikuni, M. Kinjo, A Quantitative Study of Internal and External Interactions of Homodimeric Glucocorticoid Receptor Using Fluorescence Cross-Correlation Spectroscopy in a Live Cell, *Sci. Rep.* 7 (2017) 1–16. doi:10.1038/s41598-017-04499-7.
- [27] K. Bacia, I. V. Majoul, P. Schwille, Probing the endocytic pathway in live cells using dual-color fluorescence cross-correlation analysis, *Biophys. J.* 83 (2002) 1184–1193. doi:10.1016/S0006-3495(02)75242-9.
- [28] L. Nuhn, M. Hirsch, B. Krieg, K. Koynov, K. Fischer, M. Schmidt, M. Helm, R. Zentel, Cationic nanohydrogel particles as potential siRNA carriers for cellular delivery, *ACS Nano.* 6 (2012) 2198–2214. doi:10.1021/nn204116u.

- [29] J.P. Clamme, J. Azoulay, Y. Mély, Monitoring of the formation and dissociation of polyethylenimine/DNA complexes by two photon fluorescence correlation spectroscopy, *Biophys. J.* 84 (2003) 1960–1968. doi:10.1016/S0006-3495(03)75004-8.
- [30] T. Ohrt, J. Mütze, W. Staroske, L. Weinmann, J. Höck, K. Crell, G. Meister, P. Schwille, Fluorescence correlation spectroscopy and fluorescence cross-correlation spectroscopy reveal the cytoplasmic origination of loaded nuclear RISC in vivo in human cells, *Nucleic Acids Res.* 36 (2008) 6439–6449. doi:10.1093/nar/gkn693.
- [31] A.C. Richards Grayson, A.M. Doody, D. Putnam, Biophysical and structural characterization of polyethylenimine-mediated siRNA delivery in vitro, *Pharm. Res.* 23 (2006) 1868–1876. doi:10.1007/s11095-006-9009-2.
- [32] P. Andreozzi, E. Diamanti, K.R. Py-Daniel, P.R. Cáceres-Vélez, C. Martinelli, N. Politakos, A. Escobar, M. Muzi-Falconi, R. Azevedo, S.E. Moya, Exploring the pH Sensitivity of Poly(allylamine) Phosphate Supramolecular Nanocarriers for Intracellular siRNA Delivery, *ACS Appl. Mater. Interfaces.* 9 (2017) 38242–38254. doi:10.1021/acsami.7b11132.
- [33] A.A. Metwally, C. Pourzand, I.S. Blagbrough, Efficient gene silencing by self-assembled complexes of siRNA and symmetrical fatty acid amides of spermine, *Pharmaceutics.* 3 (2011) 125–140. doi:10.3390/pharmaceutics3020125.
- [34] D.J. Gary, J. Min, Y. Kim, K. Park, Y.Y. Won, The effect of N/P ratio on the in vitro and in vivo interaction properties of pegylated poly[2-(dimethylamino)ethyl methacrylate]-based siRNA complexes, *Macromol. Biosci.* 13 (2013) 1059–1071.

doi:10.1002/mabi.201300046.

- [35] J.L. Jan Wolfgang Krieger, QuickFit 3.0. A data evaluation application for biophysics, (2015). <http://www.dkfz.de/Macromol/quickfit/>.
- [36] S. Bolte, F.P. Cordelieres, A guided tour into subcellular colocalisation analysis in light microscopy, *J. Microsc.* 224 (2006) 13–232. doi:10.1111/j.1365-2818.2006.01706.x.
- [37] N. Otsu, A Threshold Selection Method from Gray-Level Histograms, *IEEE Trans. Syst. Man. Cybern.* 9 (1979) 62–66. doi:10.1109/TSMC.1979.4310076.
- [38] K. Bacia, S.A. Kim, P. Schwille, Fluorescence cross-correlation spectroscopy in living cells, *Nat. Methods.* 3 (2006) 83–89. doi:10.1038/nmeth822.
- [39] K. Buyens, M. Meyer, E. Wagner, J. Demeester, S.C. De Smedt, N.N. Sanders, Monitoring the disassembly of siRNA polyplexes in serum is crucial for predicting their biological efficacy, *J. Control. Release.* 141 (2010) 38–41. doi:10.1016/j.jconrel.2009.08.026.
- [40] H. Najafi, S.S. Abolmaali, B. Owraangi, Y. Ghasemi, A.M. Tamaddon, Serum resistant and enhanced transfection of plasmid DNA by PEG-stabilized polyplex nanoparticles of L-histidine substituted polyethyleneimine, *Macromol. Res.* 23 (2015) 618–627. doi:10.1007/s13233-015-3074-5.
- [41] C. Madeira, L.M.S. Loura, M. Prieto, A. Fedorov, M.R. Aires-Barros, Effect of ionic strength and presence of serum on lipoplexes structure monitored by FRET, *BMC Biotechnol.* 8 (2008) 20. doi:10.1186/1472-6750-8-20.

- [42] B.K. Suh, J.; Paik, H-J.; Hwang, Ionization of PEI and PAA at Various pH's, *Bioorg. Chem.* 22 (1994) 318–327.
- [43] Y.B. Hu, E.B. Dammer, R.J. Ren, G. Wang, The endosomal-lysosomal system: From acidification and cargo sorting to neurodegeneration, *Transl. Neurodegener.* 4 (2015) 1–10. doi:10.1186/s40035-015-0041-1.
- [44] J.P. Clamme, G. Krishnamoorthy, Y. Mély, Intracellular dynamics of the gene delivery vehicle polyethylenimine during transfection: Investigation by two-photon fluorescence correlation spectroscopy, *Biochim. Biophys. Acta - Biomembr.* 1617 (2003) 52–61. doi:10.1016/j.bbamem.2003.09.002.
- [45] R. Brock, M.A. Hink, T.M. Jovin, Fluorescence correlation microscopy of cells in the presence of autofluorescence, *Biophys. J.* 75 (1998) 2547–2557. doi:10.1016/S0006-3495(98)77699-4.
- [46] N. Yoshida, M. Tamura, M. Kinjo, Fluorescence Correlation Spectroscopy: A New Tool for Probing the Microenvironment of the Internal Space of Organelles, *Single Mol.* 1 (2000) 279–283. doi:10.1002/1438-5171(200012)1:4<279::AID-SIMO279>3.0.CO;2-S.
- [47] S. Hwa Kim, J. Hoon Jeong, K. Chul Cho, S. Wan Kim, T. Gwan Park, Target-specific gene silencing by siRNA plasmid DNA complexed with folate-modified poly(ethylenimine), *J. Control. Release.* 104 (2005) 223–232. doi:10.1016/j.jconrel.2005.02.006.